Science Advances

AAAS

advances.sciencemag.org/cgi/content/full/3/11/e1701696/DC1

Supplementary Materials for

Moiré excitons: From programmable quantum emitter arrays to spin-orbit–coupled artificial lattices

Hongyi Yu, Gui-Bin Liu, Jianju Tang, Xiaodong Xu, Wang Yao

Published 10 November 2017, *Sci. Adv.* **3**, e1701696 (2017)
DOI: 10.1126/sciadv.1701696

This PDF file includes:

- fig. S7. The six reciprocal lattice vectors in the Fourier components of the excitonic potential, and the obtained hopping magnitudes $t_{0,1,2}$ as functions of the moiré period b or V/E_R.
- table S1. The parameters for fitting the first-principles results (symbols in fig. S2) with eqs. S2 and S3.
- table S2. The $\hat{C}_3$ quantum number of **K**-point Bloch function ψ_c or ψ_v^* for different rotation centers, taken from Liu *et al.* (*29*).
- table S3. The estimated radiative lifetimes for the interlayer exciton wave packets at ***A*** or ***B*** site in different heterobilayers with b = 15 nm.
- References (*48–56*)

Supplementary Text

section S1. Modulated electronic and topographic properties in the heterobilayer moiré

(1) Characterization of local interlayer atomic registry in the moiré

We consider a heterobilayer moiré pattern formed by two layers of MoX_2 and WX_2'. We denote the MoX_2 (WX_2') layer lattice constants as a (a'), and $\delta\theta$ is the small deviation angle between the zigzag crystalline axes of the two layers. For $\delta = a'/a - 1 \ll 1$ and $\delta\theta \ll 1$, the formed moiré pattern has a superlattice constant $b \approx a/\sqrt{\delta\theta^2 + \delta^2}$, which is much larger than a', a and can be tuned by changing $\delta\theta$. We set the origin for the in-plane coordinate (**R**) on a Mo atom. The locally different interlayer atomic registry in the moiré pattern can be quantified by $\mathbf{r}_0(\mathbf{R})$, the in-plane displacement vector from a nearby W atom to a Mo atom located at **R**, and without losing generality, we restrict $\mathbf{r}_0(\mathbf{R})$ to be varying within a WX_2' unit cell (fig. S1).

The function $\mathbf{r}_0(\mathbf{R})$ is a mapping from the moiré supercell to the monolayer unit cell: when **R** traverses a moiré supercell, the corresponding $\mathbf{r}_0(\mathbf{R})$ value traverses the WX_2' unit cell. Assuming no change of in-plane coordinates due to strain or topographic modulation by the moiré, $\mathbf{r}_0(\mathbf{R})$ is simply a linear function of **R**

$$\mathbf{r}_0(\mathbf{R}) = \mathbf{r}_0(0) + \mathbf{R} - \mathbf{R}' = \mathbf{r}_0(0) + l(\mathbf{a}_1 - \mathbf{a}_1') + n(\mathbf{a}_2 - \mathbf{a}_2') \qquad \text{(S1)}$$

Here $\mathbf{R} \equiv l\mathbf{a}_1 + n\mathbf{a}_2$ and $\mathbf{R}' \equiv l\mathbf{a}_1' + n\mathbf{a}_2' = (1+\delta)\hat{C}_{-\delta\theta}\mathbf{R}$, with $\mathbf{a}_{1,2}'$ ($\mathbf{a}_{1,2} = \frac{1}{1+\delta}\hat{C}_{\delta\theta}\mathbf{a}_{1,2}'$) the primitive lattice vectors in WX_2' (MoX_2), and l, n are integers. $\hat{C}_{-\delta\theta}\mathbf{R}$ means the rotation of **R** vector by $-\delta\theta$ angle. In presence of the strain and topographic modulation by moiré, the mapping $\mathbf{r}_0(\mathbf{R})$ can quantitatively deviate from Eq. (S1). The discussions in this work, nevertheless, do not rely on any quantitative detail of the mapping.

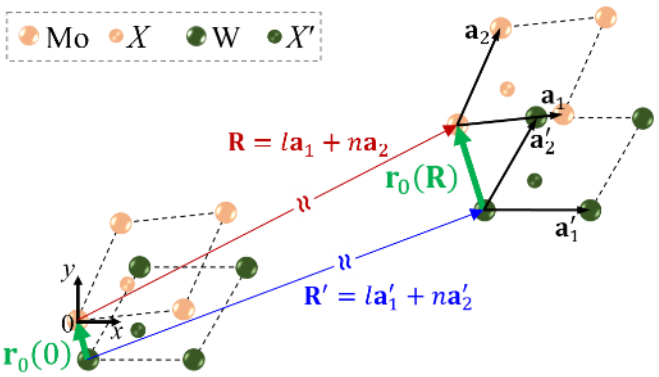

fig. S1. Schematic of how the interlayer translation vector $\mathbf{r}_0(\mathbf{R})$ (thick green arrows) changes as a function of in-plane position vector R. $\mathbf{r}_0(\mathbf{R})$ is defined as a vector pointing from a nearby W atom to the Mo atom located at R. The *xy*-coordinate origin is set on a Mo atom, where the interlayer translation is $\mathbf{r}_0(0)$.

(2) Laterally modulated local interlayer distance and local band gap

In a long period moiré pattern with $b \gg a', a$, the local interlayer separation and the local band gap are determined by the local interlayer registry $\mathbf{r}_0(\mathbf{R})$, and both of them get modulated as $\mathbf{r}_0(\mathbf{R})$ varies in the moiré, as directly revealed in STM/STS study of CVD grown MoS_2/WSe_2 heterobilayer (*26*). In length scale large compared to a', a but small compared to b, the local atomic registry at **R** (over a large number of unit cells) is nearly indistinguishable from a lattice-matched heterobilayer of (constant) interlayer registry $\mathbf{r}_0(\mathbf{R})$. The local electronic structure and interlayer distance can thus be well approximated by those of the lattice-matched bilayer, as shown by the comparison of STM/STS measured values at different locals in the MoS_2/WSe_2 moiré and the first principle calculations of lattice-matched MoS_2/WSe_2 bilayers of the corresponding $\mathbf{r}_0$, as reported in Ref. (*26*).

We have performed first-principle calculations on the interlayer separation d and band gap E_g for R- and H-type lattice-matched MoS_2/WSe_2 and $MoSe_2/WSe_2$ heterobilayers. The results are shown as the symbols in main text Fig. 1 (c,e) and fig. S2.

It is found in Ref. (*48*) that, the (local) bandgap E_g as a function of $\mathbf{r}_0$ can be well approximated by

$$E_g(\mathbf{r}_0) = E_{g,0} + \Delta E_{g,1}|f_0(\mathbf{r}_0)|^2 + \Delta E_{g,2}|f_+(\mathbf{r}_0)|^2 \qquad \text{(S2)}$$

$f_0(\mathbf{r}_0) \equiv \frac{e^{-i\mathbf{K}\cdot\mathbf{r}_0} + e^{-i\hat{C}_3\mathbf{K}\cdot\mathbf{r}_0} + e^{-i\hat{C}_3^2\mathbf{K}\cdot\mathbf{r}_0}}{3}$ and $f_\pm(\mathbf{r}_0) \equiv \frac{e^{-i\mathbf{K}\cdot\mathbf{r}_0} + e^{-i\left(\hat{C}_3\mathbf{K}\cdot\mathbf{r}_0 \pm \frac{2\pi}{3}\right)} + e^{-i\left(\hat{C}_3^2\mathbf{K}\cdot\mathbf{r}_0 \pm \frac{4\pi}{3}\right)}}{3}$ are the **K**-point coupling forms between two bands in different layers (*48*), under the two-center approximation and keeping only the leading Fourier components. This interlayer hopping affects the band gap of the type-II heterojunction through a second-order energy correction (*48*). The above equation fits our first-principle results well, as shown by the curves in Fig. 1(e) of main text and fig. S2. Interestingly, we find the interlayer separation d as function of $\mathbf{r}_0$ can also be well fitted by

$$d(\mathbf{r}_0) = d_0 + \Delta d_1 |f_0(\mathbf{r}_0)|^2 + \Delta d_2 |f_+(\mathbf{r}_0)|^2 \qquad \text{(S3)}$$

We summarize the fitting parameters in table S1.

table S1. The parameters for fitting the first-principles results (symbols in fig. S2) with eqs. S2 and S3. The constants $E_{g,0}$ have large deviations to the experimental values and are not related to the band gap modulations we are interested, thus are not shown.

	$\Delta E_{g,1}$ (eV)	$\Delta E_{g,2}$ (eV)	d_0 (Å)	Δd_1 (Å)	Δd_2 (Å)
R-type MoS_2/WSe_2	-0.116	-0.094	6.387	0.544	0.042
H-type MoS_2/WSe_2	0.058	0.072	6.919	-0.456	-0.537
R-type $MoSe_2/WSe_2$	-0.064	-0.092	6.541	0.578	0.002
H-type $MoSe_2/WSe_2$	0.014	0.026	7.082	-0.446	-0.553

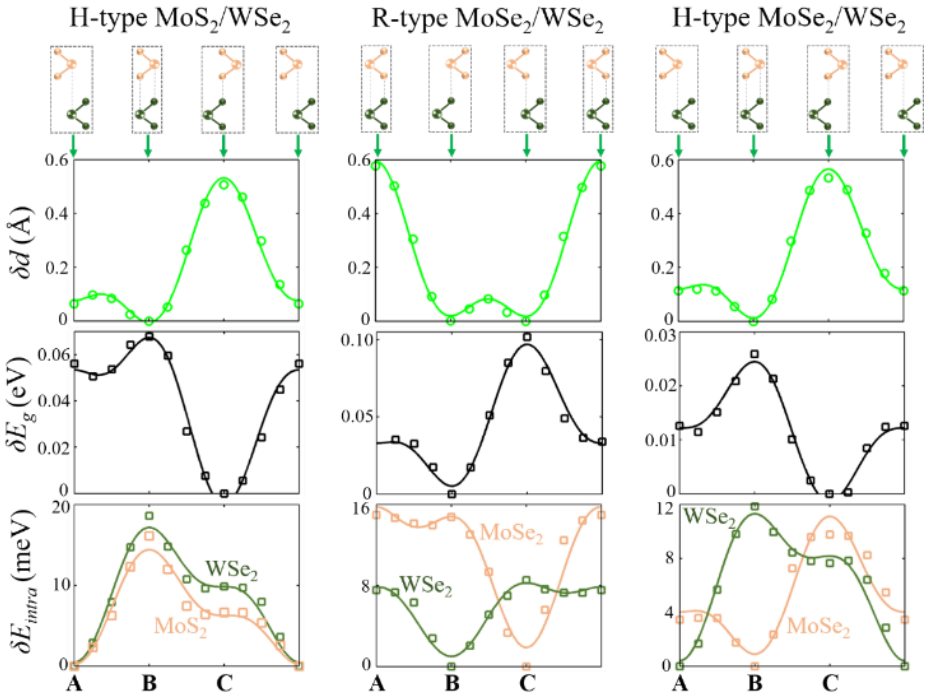

fig. S2. The modulations of layer separation δd, interlayer bandgap δE_g, and intralayer bandgap δE_{intra} for H-type MoS_2/WSe_2, R-type $MoSe_2/WSe_2$, and H-type $MoSe_2/WSe_2$ lattice-matched heterobilayers of various interlayer atomic registries. The symbols are the first-principle calculation results, while the solid lines are the fits using Eq. (S2) and (S3).

(3) Electric field tuning of potential profiles of interlayer excitons in the moiré

Electric field tuning of the potential profile of interlayer exciton in R-type MoS_2/WSe_2 heterobilayer moiré is given in Fig. 3(a)-(c) in the main text. Here we show the potential profile and field tunability of interlayer excitons in other three types of TMD heterobilayers for comparison in fig. S3.

The R-type $MoSe_2/WSe_2$ is similar to R-type MoS_2/WSe_2 (fig. S3(a)). At $\mathcal{E} = -\mathcal{E}_0$, $\mathcal{E}_0 \approx 0.49\ \mathrm{V/nm}$, a honeycomb superlattice with zero Dirac mass is realized, and the barrier height between the nearest-neighbor **A** and **B** sites is comparable to that in R-type MoS_2/WSe_2.

For H-type MoS_2/WSe_2, the exciton potential profile is a triangular superlattice over a large range of positive and negative $\mathcal{E}$ (fig. S3(b)), with the depth of the potential (δV) continuously tunable by $\mathcal{E}$.

In H-type $MoSe_2/WSe_2$, electric field can tune the potential from rather deep confinement of $\delta V > 40$ meV, to a nearly flat landscape with $\delta V \sim 7$ meV where excitons become itinerant.

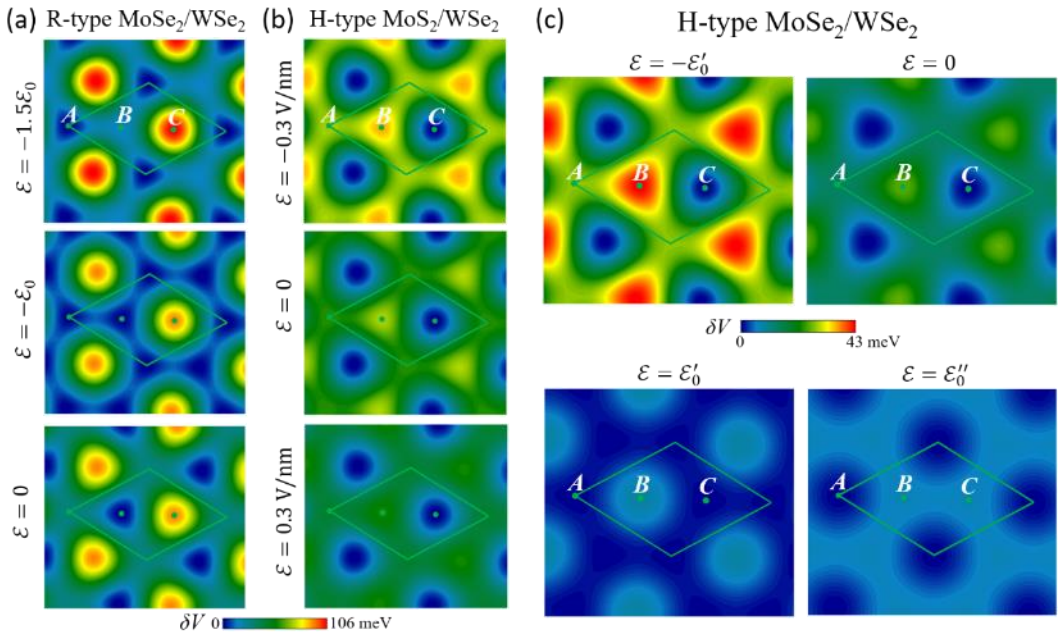

fig. S3. The potential profile of the interlayer excitons in the three types of TMD heterobilayers (see Eq. 1 in the main text). We have neglected the dependence of exciton binding energy on **R** which is expected to be weak. (a) R-type $MoSe_2/WSe_2$ ($\mathcal{E}_0 \approx 0.49\ \mathrm{V/nm}$), (b) H-type MoS_2/WSe_2 and (c) H-type $MoSe_2/WSe_2$ ($\mathcal{E}_0' \approx 0.31\ \mathrm{V/nm}$ and $\mathcal{E}_0'' \approx 0.47\ \mathrm{V/nm}$).

(4) First principle calculated optical transition matrix elements in lattice-matched bilayers

We have performed *ab initio* calculations for the direct interband optical matrix element $\mathbf{p}_{cv}$ from the valence band edge at **K**-point (predominantly in WX_2' layer) to the conduction band edge at **K**/-**K** (predominantly in MoX_2 layer), for R/H-type lattice-matched MoX_2/WX_2' heterobilayers. Its left- (right-) handed circularly polarized component $|\mathbf{e}_+ \cdot \mathbf{p}_{cv}|$ ($|\mathbf{e}_- \cdot \mathbf{p}_{cv}|$) is shown as red (blue) symbols at various interlayer registry $\mathbf{r}_0$ in fig. S4. The interlayer exciton's optical transition dipole strength is proportional to $\mathbf{p}_{cv}$. Under the two-center approximation and keeping only the leading Fourier components, it has been shown in Ref. (*28*) that the $\mathbf{r}_0$ dependence of $\mathbf{p}_{cv}$ can be described by

$$\mathbf{p}_{\mathrm{cv}} = f_0(\mathbf{r}_0)p_+(d)\mathbf{e}_+ + f_+(\mathbf{r}_0)p_-(d)\mathbf{e}_- \qquad \text{(S4)}$$

In the heterobilayer moiré, since the interlayer distance d also depends $\mathbf{r}_0$ (see Eq. (S3) and fig. S2), the $p_\pm(d)$ factors in Eq. (S4) also contribute to $\mathbf{r}_0$ dependence of $\mathbf{p}_{\mathrm{cv}}$ in the moiré. Together with Eq. (S3), the $\mathbf{r}_0$-dependences of the transition dipole $\mathbf{e}_\pm$-components in the heterobilayer moiré are expected to have the forms

$$|\mathbf{e}_+ \cdot \mathbf{p}_{\mathrm{cv}}| \approx p_+(d_0)|f_0(\mathbf{r}_0)| + \frac{\partial p_+}{\partial d}\Big|_{d=d_0} (\Delta d_1 |f_0(\mathbf{r}_0)|^2 + \Delta d_2 |f_+(\mathbf{r}_0)|^2)|f_0(\mathbf{r}_0)|,$$
$$|\mathbf{e}_- \cdot \mathbf{p}_{\mathrm{cv}}| \approx p_-(d_0)|f_+(\mathbf{r}_0)| + \frac{\partial p_-}{\partial d}\Big|_{d=d_0} (\Delta d_1 |f_0(\mathbf{r}_0)|^2 + \Delta d_2 |f_+(\mathbf{r}_0)|^2)|f_+(\mathbf{r}_0)| \qquad \text{(S5)}$$

Eq. (S5) fit well the first principle calculated $\mathbf{p}_{\mathrm{cv}}$ in lattice-matched heterobilayers of various $\mathbf{r}_0$ (solid curves in fig. S4). From fig. S4, it is clear that at the high symmetry stacking **A** or **B**, the spin up interlayer excitons (hole in $\mathbf{K}'$-valley) couple respectively to $\sigma+$ or $\sigma-$ polarized photons only, while they are dark at the high symmetry **C** stacking. This comes from the $\hat{C}_3$ ($2\pi/3$-rotational) symmetry of such stacking.

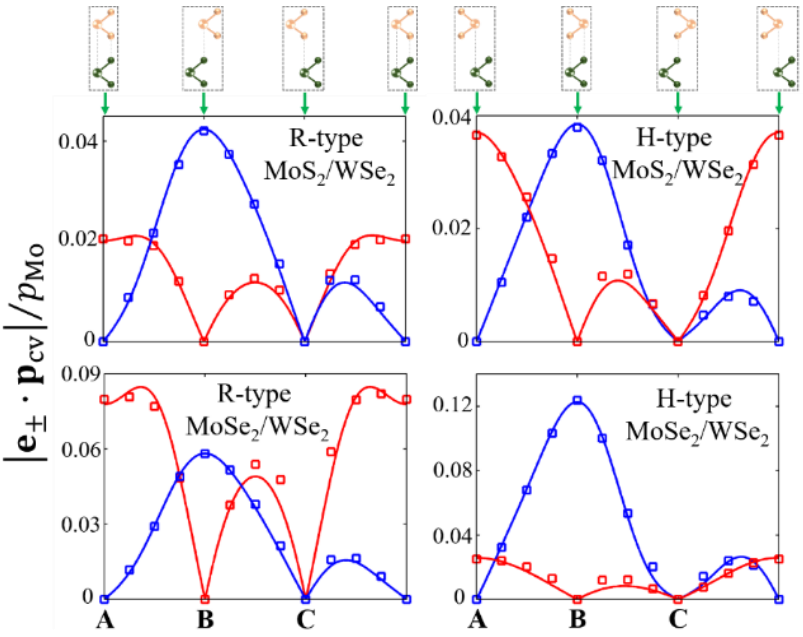

fig. S4. The ab initio results of the optical matrix elements at various interlayer translations $\mathbf{r}_0$. The red and blue symbols are the *ab initio* results of $|\mathbf{e}_+ \cdot \mathbf{p}_{\mathrm{cv}}|$ and $|\mathbf{e}_- \cdot \mathbf{p}_{\mathrm{cv}}|$, respectively, at various interlayer translation $\mathbf{r}_0$. p_{Mo} is the magnitude of the **K**-point *intralayer* optical matrix element between the valence and conduction bands in the MoX_2 layer, which is proportional to the intralayer exciton transition dipole. The solid curves are the fits using Eq. (S5), each with two fitting parameters $p_\pm(d_0)$ and $\frac{\partial p_\pm}{\partial d}\big|_{d=d_0}$, while other parameters involved are from table S1.

section S2. Nanopatterned optical properties of the interlayer excitons in the moiré

MX_2 monolayers have conduction and valence band edges at **K** and -**K** corners of the hexagonal Brillouin zone (BZ), where large spin-orbit splitting leads to an effective locking of spin to valley, i.e. the valence band edge at **K** (-**K**) has spin up (down) states only. Optically active excitons thus have a spin-1/2 spanned by the spin-valley locked band edges. In the analysis hereafter, we use spin up interlayer excitons in R-type heterobilayers (therefore electron in **K**-valley and hole in $\mathbf{K}'$-valley) as examples to demonstrate the optical properties. Those in H-type heterobilayers can be obtained similarly, and results are directly presented.

(1) Interlayer exciton in the wavepacket form

The momentum eigenstates of interlayer excitons in the presence of lattice mismatch have been derived in Ref. (*28*)

$$X_{\mathbf{Q}}(\mathbf{r}_{\mathrm{e}},\mathbf{r}_{\mathrm{h}})=\sum_{\Delta\mathbf{Q}}\Phi(\Delta\mathbf{Q})\psi_{\frac{m_{\mathrm{e}}}{M_0}\mathbf{Q}+\Delta\mathbf{Q},\mathrm{c}}(\mathbf{r}_{\mathrm{e}})\psi^{*}_{-\frac{m_{\mathrm{h}}}{M_0}\mathbf{Q}+\Delta\mathbf{Q},\mathrm{v}}(\mathbf{r}_{\mathrm{h}}) \qquad \text{(S6)}$$

Here $\psi_{\mathbf{k},\mathrm{c}}(\mathbf{r}_{\mathrm{e}})=e^{i(\mathbf{K}+\mathbf{k})\cdot\mathbf{r}_{\mathrm{e}}}u_{\mathbf{k},\mathrm{c}}(\mathbf{r}_{\mathrm{e}})$ ($\psi_{\mathbf{k}',\mathrm{v}}(\mathbf{r}_{\mathrm{h}})=e^{i(\mathbf{K}'+\mathbf{k}')\cdot\mathbf{r}_{\mathrm{h}}}u_{\mathbf{k}',\mathrm{v}}(\mathbf{r}_{\mathrm{h}})$) is the conduction (valence) electron Bloch function with wave vector $\mathbf{K}+\mathbf{k}$ ($\mathbf{K}'+\mathbf{k}'$), and $u_{\mathbf{k},\mathrm{c}}$ ($u_{\mathbf{k}',\mathrm{v}}$) is the period part. $M_0\equiv m_{\mathrm{e}}+m_{\mathrm{h}}$ is the exciton mass, with m_{e} (m_{h}) the electron (hole) effective mass. $\Phi(\Delta\mathbf{Q})$ describes the **k**-space electron-hole relative motion. As shown in Ref. (*28*), $X_{\mathbf{Q}}(\mathbf{r}_{\mathrm{e}},\mathbf{r}_{\mathrm{h}})$ is the eigenstate of kinetic energy, with eigenvalue $E_{\mathbf{Q}}=\frac{\hbar^2|\mathbf{Q}|^2}{2M_0}$, so the index **Q** corresponds to the *kinematic* momentum: $\langle X_{\mathbf{Q}}|\dot{\mathbf{R}}_X|X_{\mathbf{Q}}\rangle\equiv\langle X_{\mathbf{Q}}|\frac{m_{\mathrm{e}}}{M_0}\dot{\mathbf{r}}_{\mathrm{e}}+\frac{m_{\mathrm{h}}}{M_0}\dot{\mathbf{r}}_{\mathrm{h}}|X_{\mathbf{Q}}\rangle=\frac{\hbar}{M_0}\mathbf{Q}$, with $\mathbf{R}_X\equiv\frac{m_{\mathrm{e}}}{M_0}\mathbf{r}_{\mathrm{e}}+\frac{m_{\mathrm{h}}}{M_0}\mathbf{r}_{\mathrm{h}}$ the exciton center-of-mass (COM) coordinate.

In the presence of superlattice potential due to the moiré modulated local band gap and interlayer distance (Eq. (1) in the main text), the description of optical properties of interlayer excitons can be facilitated by wavepackets moving adiabatically in the periodic potential. The momentum eigenstates in Eq. (S6) can serve as a basis to construct the wavepackets. Here and hereafter we consider low energy interlayer excitons only, where the electron-hole relative motion is always in the ground state. An exciton wavepacket centered at **R** is given by

$$\mathcal{X}_{\mathbf{R}}=\sum_{\mathbf{Q}}e^{-i(\mathbf{Q}+\mathbf{K}-\mathbf{K}')\cdot\mathbf{R}}W(\mathbf{Q})X_{\mathbf{Q}}(\mathbf{r}_{\mathrm{e}},\mathbf{r}_{\mathrm{h}}) \qquad \text{(S7)}$$

Here $W(\mathbf{Q}) = \sqrt{\frac{4\pi}{S}} w e^{-w^2\mathbf{Q}^2/2}$, normalized such that $\sum_{\mathbf{Q}} |W(\mathbf{Q})|^2 = \frac{S}{(2\pi)^2} \int |W(\mathbf{Q})|^2 d\mathbf{Q} = 1$ with S the box normalization area. w corresponds to the real space extension of the exciton COM wavefunction, which shall be small compared to the moiré period b.

(2) Light coupling of interlayer exciton wavepackets at high-symmetry locations

Here we consider an interlayer exciton wavepacket $\mathcal{X}_{\mathbf{R}}$ at the high-symmetry location **A**, **B** or **C** (see Fig. 1(a) in the main text), which has the $2\pi/3$-rotational ($\hat{C}_3$) symmetry around its center **R**. The $\hat{C}_3$ quantum number of such an exciton is determined by both the **K**-point electron Bloch state $\psi_{\mathrm{c}}(\mathbf{r}_{\mathrm{e}})$ and $\mathbf{K}'$-point hole Bloch state $\psi_{\mathrm{v}}^*(\mathbf{r}_{\mathrm{h}})$, which mainly consist of metal atom $d_{m=0} \equiv d_{z^2}$ and $d_{m=+2} \equiv \frac{d_{x^2-y^2 \pm i d_{xy}}}{\sqrt{2}}$ orbitals, respectively. The Bloch states have the forms

$$\psi_{\mathrm{c}}(\mathbf{r}_{\mathrm{e}}) = \frac{1}{\sqrt{N}} \sum_n e^{i\mathbf{K}\cdot\mathbf{R}_n} d_{m=0}(\mathbf{r}_{\mathrm{e}} - \mathbf{R}_n)$$

$$\psi_{\mathrm{v}}(\mathbf{r}_{\mathrm{h}}) = \frac{1}{\sqrt{N'}} \sum_n e^{i\mathbf{K}'\cdot\mathbf{R}'_n} d_{m=+2}(\mathbf{r}_{\mathrm{h}} - \mathbf{R}'_n)$$

Here N (N') is the lattice site number of the Mo (W) layer, and $\mathbf{R}_n$ ($\mathbf{R}'_n$) is the coordinate of the nth metal site. Under $2\pi/3$-rotations, both the phase factors ($e^{i\mathbf{K}\cdot\mathbf{R}_n}$ and $e^{i\mathbf{K}'\cdot\mathbf{R}'_n}$) and the d_m orbitals contribute to the resulted $\hat{C}_3$ quantum numbers. The contribution from $e^{i\mathbf{K}\cdot\mathbf{R}_n}$ and $e^{i\mathbf{K}'\cdot\mathbf{R}'_n}$ depends on the choice of rotation center. Thus the overall $\hat{C}_3$ eigenvalues of ψ_{c} and ψ_{v}^* are also rotation center dependent, as summarized in table S2 below. The combined $\hat{C}_3$ eigenvalue of the electron-hole pair $\psi_{\mathrm{c}}\psi_{\mathrm{v}}^*$ in the same layer has no dependence on the choice of rotation center, which determines the optical selection rule of *intralayer* transition.

table S2. The $\hat{C}_3$ quantum number of K-point Bloch function ψ_c or ψ_v^* for different rotation centers, taken from Liu *et al.* (*29*). h (hexagon center), M (metal site), or X (chalcogen site).

	h	X	M
ψ_{c}	$e^{-i2\pi/3}$	$e^{i2\pi/3}$	1
ψ_{v}^*	1	$e^{i2\pi/3}$	$e^{-i2\pi/3}$

For interlayer exciton in the heterobilayer, the interlayer registry thus matters. We can fix the rotation on an h center of the hole layer, so the hole wavefunction transforms as $\hat{C}_3\psi_{\mathrm{v}}^* = \psi_{\mathrm{v}}^*$. The $\hat{C}_3$ eigenvalue of interlayer exciton is then that of the electron about the common rotation center.

At **A**, **B** and **C** locals in the moiré supercell, the h centers of the hole layer correspond to h, X and M of the electron layer, respectively. From table S2 we have

$$\hat{C}_3\mathcal{X}_{\mathbf{A}} = e^{-i2\pi/3}\mathcal{X}_{\mathbf{A}}, \qquad \hat{C}_3\mathcal{X}_{\mathbf{B}} = e^{i2\pi/3}\mathcal{X}_{\mathbf{B}}, \qquad \hat{C}_3\mathcal{X}_{\mathbf{C}} = \mathcal{X}_{\mathbf{C}} \tag{S8}$$

which is Eq. (2) in the main text for the spin up exciton (s = +). Eq. (S8) is a consequence of the different interlayer registry at these high symmetry locals. Different choices of hole rotation center lead to the same conclusion.

When the exciton radiatively recombines, the emitted photon must have the same $\hat{C}_3$ eigenvalue with the exciton. Eq. (S8) then implies that, the exciton wavepacket $\mathcal{X}_{\mathbf{A}}$ ($\mathcal{X}_{\mathbf{B}}$) couples to $\sigma+$ ($\sigma-$) circularly polarized photon, while light coupling is forbidden for $\mathcal{X}_{\mathbf{C}}$.

(3) Light coupling of interlayer exciton wavepackets at general locations

The light coupling properties of an exciton wavepacket $\mathcal{X}_{\mathbf{R}}$ is characterized by its optical transition dipole $\boldsymbol{\mathcal{D}}(\mathbf{R})$, which from Eq. (S7) can be obtained from the transition dipole $\mathbf{D}_{\mathbf{Q}}$ of momentum eigenstate $X_{\mathbf{Q}}(\mathbf{r}_{\mathrm{e}}, \mathbf{r}_{\mathrm{h}})$ that has been derived in Ref. (*28*). Under the two-center approximation and keeping only the leading Fourier components, $\mathbf{D}_{\mathbf{Q}}$ can be written as (*28*)

$$\begin{aligned}\mathbf{D}_{\mathbf{Q}} = &\left(\delta_{\mathbf{Q},\mathbf{Q}_0}e^{-i\mathbf{K}'\cdot\mathbf{r}_0(0)} + \delta_{\mathbf{Q},\hat{C}_3\mathbf{Q}_0}e^{-i\hat{C}_3\mathbf{K}'\cdot\mathbf{r}_0(0)} + \delta_{\mathbf{Q},\hat{C}_3^2\mathbf{Q}_0}e^{-i\hat{C}_3^2\mathbf{K}'\cdot\mathbf{r}_0(0)}\right)\frac{D_+(d)}{3}\mathbf{e}_+ \\ &+\left(\delta_{\mathbf{Q},\mathbf{Q}_0}e^{-i\mathbf{K}'\cdot\mathbf{r}_0(0)} + \delta_{\mathbf{Q},\hat{C}_3\mathbf{Q}_0}e^{-i\left(\hat{C}_3\mathbf{K}'\cdot\mathbf{r}_0(0)+\frac{2\pi}{3}\right)} + \delta_{\mathbf{Q},\hat{C}_3^2\mathbf{Q}_0}e^{-i\left(\hat{C}_3^2\mathbf{K}'\cdot\mathbf{r}_0(0)+\frac{4\pi}{3}\right)}\right)\frac{D_-(d)}{3}\mathbf{e}_-\end{aligned} \tag{S9}$$

Here the $\mathbf{e}_\pm \equiv \frac{\mathbf{x}\pm i\mathbf{y}}{\sqrt{2}}$ component couples to $\sigma\pm$ circularly polarized photon. $D_\pm(d)$ are two real values proportional to $p_\pm(d)$ in Eq. (S4) which decay with the interlayer distance d. $\mathbf{Q}_0 \equiv \mathbf{K}' - \mathbf{K}$, $\hat{C}_3\mathbf{Q}_0$ and $\hat{C}_3^2\mathbf{Q}_0$ are the three corners of the moiré-BZ, at which exciton momentum eigenstates can interconvert with photons directly (satisfying momentum conservation) (*28*).

From Eq. (S9) and Eq. (S7), we find the optical transition dipole of an exciton wavepacket

$$\begin{aligned}\boldsymbol{\mathcal{D}}(\mathbf{R}) &= e^{i\mathbf{Q}_0\cdot\mathbf{R}}\sum_{\mathbf{Q}} e^{-i\mathbf{Q}\cdot\mathbf{R}}W(\mathbf{Q})\mathbf{D}_{\mathbf{Q}} \\ &= e^{i\mathbf{Q}_0\cdot\mathbf{R}}W(\mathbf{Q}_0)\left[\left(e^{-i\left(\mathbf{Q}_0\cdot\mathbf{R}+\mathbf{K}'\cdot\mathbf{r}_0(0)\right)} + e^{-i\left(\hat{C}_3\mathbf{Q}_0\cdot\mathbf{R}+\hat{C}_3\mathbf{K}'\cdot\mathbf{r}_0(0)\right)} + e^{-i\left(\hat{C}_3^2\mathbf{Q}_0\cdot\mathbf{R}+\hat{C}_3^2\mathbf{K}'\cdot\mathbf{r}_0(0)\right)}\right)\frac{D_+(d)}{3}\mathbf{e}_+\right. \\ &\quad\left.+\left(e^{-i\left(\mathbf{Q}_0\cdot\mathbf{R}+\mathbf{K}'\cdot\mathbf{r}_0(0)\right)} + e^{-i\left(\hat{C}_3\mathbf{Q}_0\cdot\mathbf{R}+\hat{C}_3\mathbf{K}'\cdot\mathbf{r}_0(0)+\frac{2\pi}{3}\right)} + e^{-i\left(\hat{C}_3^2\mathbf{Q}_0\cdot\mathbf{R}+\hat{C}_3^2\mathbf{K}'\cdot\mathbf{r}_0(0)+\frac{4\pi}{3}\right)}\right)\frac{D_-(d)}{3}\mathbf{e}_-\right]\end{aligned} \tag{S10}$$

The requirement of a small wavepacket extension in real space ($w \ll b = \frac{4\pi}{3|\mathbf{Q}_0|}$) is equivalent to $1/w \gg |\mathbf{Q}_0|$, i.e., the wavepacket extension in $\mathbf{Q}$-space ($1/w$) is much larger than the moiré-BZ size (fig. S5). Thus $W(\mathbf{Q}_0) \approx W(0) = \sqrt{\frac{4\pi}{S}}w$, such a wavepacket has a finite transition dipole given by the interference of those $\mathbf{D}_\mathbf{Q}$ at the three corners $\mathbf{Q}_0$, $\hat{C}_3\mathbf{Q}_0$ and $\hat{C}_3^2\mathbf{Q}_0$.

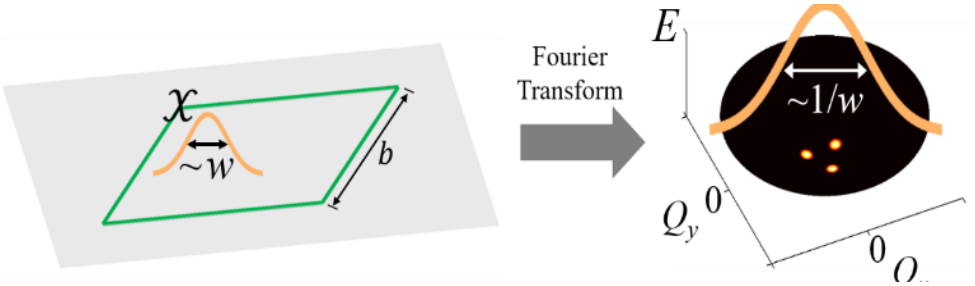

fig. S5. The real-space form of an interlayer exciton wave packet χ, with width $w \ll b$, corresponds to a Q-space distribution covering all the three main light cones (bright spots).

The phases in Eq. (S10) can be expressed as

$$\begin{aligned}\mathbf{Q}_0 \cdot \mathbf{R} + \mathbf{K}' \cdot \mathbf{r}_0(0) &= (\mathbf{K}' - \mathbf{K}) \cdot (l\mathbf{a}_1 + n\mathbf{a}_2) + \mathbf{K}' \cdot \mathbf{r}_0(0) \\ &= \mathbf{K}' \cdot \big((l\mathbf{a}_1 + n\mathbf{a}_2) - (l\mathbf{a}_1' + n\mathbf{a}_2')\big) + \mathbf{K}' \cdot \mathbf{r}_0(0) = \mathbf{K}' \cdot \mathbf{r}_0(\mathbf{R})\end{aligned}$$

where the last step has used Eq. (S1). Similarly $\hat{C}_3\mathbf{Q}_0 \cdot \mathbf{R} + \hat{C}_3\mathbf{K}' \cdot \mathbf{r}_0(0) = \hat{C}_3\mathbf{K}' \cdot \mathbf{r}_0(\mathbf{R})$ and $\hat{C}_3^2\mathbf{Q}_0 \cdot \mathbf{R} + \hat{C}_3^2\mathbf{K}' \cdot \mathbf{r}_0(0) = \hat{C}_3^2\mathbf{K}' \cdot \mathbf{r}_0(\mathbf{R})$. So the transition dipole of the wavepacket is exclusively determined by $\mathbf{r}_0(\mathbf{R})$, the interlayer translation at the wavepacket center

$$\begin{aligned}\boldsymbol{\mathcal{D}}(\mathbf{R}) \approx e^{i\mathbf{Q}_0\cdot\mathbf{R}}\sqrt{\frac{4\pi}{S}}w\Big[&\Big(e^{-i\mathbf{K}'\cdot\mathbf{r}_0(\mathbf{R})} + e^{-i\hat{C}_3\mathbf{K}'\cdot\mathbf{r}_0(\mathbf{R})} + e^{-i\hat{C}_3^2\mathbf{K}'\cdot\mathbf{r}_0(\mathbf{R})}\Big)\frac{D_+(d)}{3}\mathbf{e}_+ \\ &+ \Big(e^{-i\mathbf{K}'\cdot\mathbf{r}_0(\mathbf{R})} + e^{-i\left[\hat{C}_3\mathbf{K}'\cdot\mathbf{r}_0(\mathbf{R})+\frac{2\pi}{3}\right]} + e^{-i\left[\hat{C}_3^2\mathbf{K}'\cdot\mathbf{r}_0(\mathbf{R})+\frac{4\pi}{3}\right]}\Big)\frac{D_-(d)}{3}\mathbf{e}_-\Big]\end{aligned} \quad \text{(S11)}$$

This equation is analogous to the transition dipole in a lattice-matched heterobilayer (Eq. (S4)), except that the constant interlayer translation vector $\mathbf{r}_0$ there is now replaced by the location-dependent local value $\mathbf{r}_0(\mathbf{R})$ in the moiré. Eq. (S11) shows that the optical properties of the exciton wavepacket is determined by the local atomic registry within the wavepacket extension, thus vary continuously with the central position $\mathbf{R}$ of the wavepacket, as shown in main text Fig.

2 for the R-type MoS_2/WSe_2 moiré. The symmetry dictated results in Eq. (S8) are well reproduced. At a general local in the moiré where the local interlayer registry no longer observes the $\hat{C}_3$ symmetry, the photon emission is of the general elliptical polarization. In fig. S6, the results in H-type MoS_2/WSe_2 moiré are also given, which show similar nano-patterned optical properties.

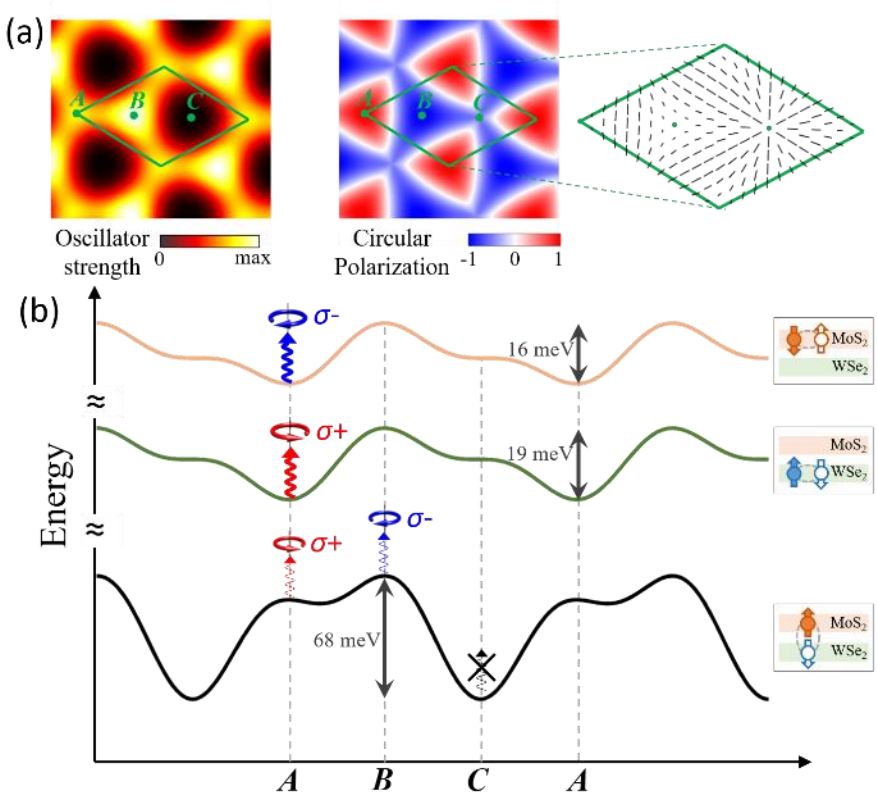

fig. S6. Nanopatterned spin optics of moiré excitons in an H-type MoS_2/WSe_2 moiré pattern. (a) Left: Oscillator strength of interlayer exciton wavepackets in a near H-type MoS_2/WSe_2 moiré pattern. Right: Optical selection rule for interlayer exciton wavepackets with the hole in $\mathbf{K}'$ valley and electron in $-\mathbf{K}$ valley. (b) From up to down: superlattice potential for $-\mathbf{K}$ valley intralayer excitons in MoS_2, $\mathbf{K}'$ valley intralayer excitons in WSe_2, and interlayer excitons with the hole in $\mathbf{K}'$ valley and electron in $-\mathbf{K}$ valley. The optical selection rules for intralayer and interlayer exciton wavepackets centered at **A**, **B** and **C** are also shown.

*(4) Radiative lifetime of an interlayer exciton in the nanodots confinement at **A** & **B***

The radiative lifetime of an intralayer exciton wavepacket in monolayer TMDs has been derived in Ref. (*49*). Here we use the same approach to estimate the radiative lifetime of an interlayer exciton wavepacket. For the wavepacket located at $\mathbf{R}$, its radiative lifetime $\mathcal{T}(\mathbf{R})$ is given by

$$\mathcal{T}(\mathbf{R}) \approx \frac{\tau_{\mathbf{R}}(\mathbf{k}=0)}{(w\omega/c)^2}$$

Here $\hbar\omega\sim1$ eV ($\sim$1.4 eV) is the emitted photon energy in heterobilayer MoS_2/WSe_2 (*26*) ($MoSe_2/WSe_2$ (*16*)). $\tau_{\mathbf{R}}(\mathbf{k}=0)$ is the radiative lifetime of an interlayer exciton at zero COM wave vector in a lattice-matched heterobilayer ($\mathbf{Q}_0=0$) of the corresponding interlayer distance d and interlayer translation $\mathbf{r}_0$.

Note that the emission rate $\left(\tau_{\mathbf{R}}(\mathbf{k}=0)\right)^{-1}$ is proportional to the square of the interlayer exciton transition dipole $|\mathbf{D}_{\mathbf{k}=0}|^2$, thus $\frac{\tau_{\mathbf{R}}(\mathbf{k}=0)}{\tau_{\mathrm{intra}}}=\left(\frac{D_{\mathrm{intra}}}{|\mathbf{D}_{\mathbf{k}=0}|}\right)^2$ where τ_{intra} is the radiative lifetime of the intralayer exciton in the light cone and D_{intra} is the corresponding transition dipole strength. The various literatures have consistently suggested a sub-picosecond τ_{intra} in monolayer TMDs, and here we take $\tau_{\mathrm{intra}}\sim0.15$ ps as measured in Ref. (*50*). $\frac{|\mathbf{D}_{\mathbf{k}=0}|}{D_{\mathrm{intra}}}\approx\frac{|\mathbf{p}_{\mathrm{cv}}|}{p_{\mathrm{Mo}}}$ has been given in fig. S4, and the calculated values are consistent with the observation that interlayer exciton oscillator strength is two to three orders of magnitude smaller than that of the intralayer exciton (*51*).

For the interlayer exciton in the ground state of the nanodot confinement at **A** or **B**, we estimate the wavepacket extension $w\approx0.3b$ (*35*). For a moiré superlattice with period $b=15$ nm, the estimated lifetime $\mathcal{T}$ at **A** and **B** sites is given in table S3. With the change of b, the lifetime scales as $\mathcal{T}(\mathbf{R})\propto b^{-2}$.

table S3. The estimated radiative lifetimes for the interlayer exciton wave packets at *A* or *B* site in different heterobilayers with *b* = 15 nm.

	R-MoS_2/WSe_2	H-MoS_2/WSe_2	R-$MoSe_2/WSe_2$	H-$MoSe_2/WSe_2$
A	80 ns	20 ns	3 ns	30 ns
B	20 ns	20 ns	5 ns	1 ns

section S3. Complex hopping of the interlayer excitons in the moiré

In the main text we have obtained the phase of the hopping amplitude between two wavepackets centered at **A** and **B** sites, respectively, based on the $\hat{C}_3$ quantum number of the exciton wavepacket dictated by the local atomic registry (Eq. (S8)). Here we derive the complex hopping between two general locations in the moiré.

Under envelope approximation for the electron and hole Bloch functions $\psi_{\mathbf{k},\mathrm{c}}(\mathbf{r}_\mathrm{e})\approx e^{i(\mathbf{K}+\mathbf{k})\cdot\mathbf{r}_\mathrm{e}}u_{\mathbf{k}=0,\mathrm{c}}(\mathbf{r}_\mathrm{e})$, $\psi_{\mathbf{k}',\mathrm{v}}(\mathbf{r}_\mathrm{h})\approx e^{i(\mathbf{K}'+\mathbf{k}')\cdot\mathbf{r}_\mathrm{h}}u_{\mathbf{k}'=0,\mathrm{v}}(\mathbf{r}_\mathrm{h})$, the exciton momentum eigenstate in Eq. (S6) becomes

$$X_{\mathbf{Q}}(\mathbf{r}_\mathrm{e},\mathbf{r}_\mathrm{h})\approx e^{i\mathbf{Q}\cdot\mathbf{R}_X}e^{i(\mathbf{K}-\mathbf{K}')\cdot\mathbf{R}_X}\Phi(\mathbf{r}_{\mathrm{eh}})u_{\mathbf{k}=0,\mathrm{c}}(\mathbf{r}_\mathrm{e})u^*_{\mathbf{k}'=0,\mathrm{v}}(\mathbf{r}_\mathrm{h}) \qquad \text{(S12)}$$

where $\Phi(\mathbf{r}_{\rm eh}) \equiv \sum_{\Delta\mathbf{Q}} \Phi(\Delta\mathbf{Q}) e^{i\left(\Delta\mathbf{Q}+\frac{m_{\rm h}}{M_0}\mathbf{K}+\frac{m_{\rm e}}{M_0}\mathbf{K}'\right)\cdot\mathbf{r}_{\rm eh}}$ is the envelope function for the electron-hole relative motion (in the ground state of relative motion only), and $\mathbf{r}_{\rm eh} \equiv \mathbf{r}_{\rm e} - \mathbf{r}_{\rm h}$ is the electron-hole relative coordinate. The exciton wavepacket in Eq. (S7) can then be written as

$$\mathcal{X}_{\mathbf{R}}(\mathbf{r}_{\rm e}, \mathbf{r}_{\rm h}) \approx e^{i(\mathbf{K}-\mathbf{K}')\cdot(\mathbf{R}_X-\mathbf{R})} W(\mathbf{R}_X - \mathbf{R}) \Phi(\mathbf{r}_{\rm eh}) u_{\mathbf{k}=0,{\rm c}}(\mathbf{r}_{\rm e}) u^*_{\mathbf{k}'=0,{\rm v}}(\mathbf{r}_{\rm h}) \qquad \text{(S13)}$$

where $W(\mathbf{R}_X - \mathbf{R}) = \frac{1}{w\sqrt{\pi}} e^{-(\mathbf{R}_X-\mathbf{R})^2/2w^2}$. The hopping integral of a wavepacket from site $\mathbf{R}_1$ to $\mathbf{R}_2$ is then

$$\begin{aligned} t(\mathbf{R}_2 - \mathbf{R}_1) &\equiv \int \mathcal{X}^*_{\mathbf{R}_2}(\mathbf{r}_{\rm e}, \mathbf{r}_{\rm h}) \widehat{H}_T \mathcal{X}_{\mathbf{R}_1}(\mathbf{r}_{\rm e}, \mathbf{r}_{\rm h}) d\mathbf{r}_{\rm e} d\mathbf{r}_{\rm h} \qquad \text{(S14)} \\ &\cong e^{i(\mathbf{K}-\mathbf{K}')\cdot(\mathbf{R}_2-\mathbf{R}_1)} \int W^*(\mathbf{R}_X - \mathbf{R}_2) \widehat{H}_T W(\mathbf{R}_X - \mathbf{R}_1) d\mathbf{R}_X \int |\Phi(\mathbf{r}_{\rm eh})|^2 d\mathbf{r}_{\rm eh} \end{aligned}$$

where $\widehat{H}_T$ is the Hamiltonian for the exciton COM motion in the superlattice potential. In the last step of Eq. (S14), we have separated out the fast oscillating component $u_{\rm c}(\mathbf{r}_{\rm e}) u^*_{\rm v}(\mathbf{r}_{\rm h})$ from the exciton envelope function that is varying in the much larger length scale of exciton Bohr radius and wavepacket width *w*.

Since $\int W^*(\mathbf{R}_X - \mathbf{R}_2) \widehat{H}_T W(\mathbf{R}_X - \mathbf{R}_1) d\mathbf{R}_X$ is real, the hopping integral $t(\mathbf{R}_2 - \mathbf{R}_1)$ has the phase factor of $e^{i(\mathbf{K}-\mathbf{K}')\cdot(\mathbf{R}_2-\mathbf{R}_1)}$. This result is fully consistent with the symmetry dictated phases of the nearest-neighbor (third nearest-neighbor) hopping between **A** and **B** sites (c.f. main text Eq. (3) and Fig. 4(a)). In the nearest-neighbor (third nearest-neighbor) hopping, the displacement vector $\mathbf{R}_2 - \mathbf{R}_1$ equals $\mathbf{d}_0 \equiv \frac{b}{\sqrt{3}}(1,0)$, $\hat{C}_3\mathbf{d}_0$ or $\hat{C}_3^2\mathbf{d}_0$ ($\mathbf{d}_2 \equiv \frac{2b}{\sqrt{3}}(-1,0)$, $\hat{C}_3\mathbf{d}_2$ or $\hat{C}_3^2\mathbf{d}_2$), so the hopping phase factors are then $e^{i(\mathbf{K}-\mathbf{K}')\cdot\mathbf{d}_{0/2}} = 1$, $e^{i(\mathbf{K}-\mathbf{K}')\cdot\hat{C}_3\mathbf{d}_{0/2}} = e^{-i4\pi/3}$ or $e^{i(\mathbf{K}-\mathbf{K}')\cdot\hat{C}_3^2\mathbf{d}_{0/2}} = e^{i4\pi/3}$. Note that $\mathbf{K} - \mathbf{K}' = \frac{4\pi}{3b}(0,1)$ in main text Fig. 4(a). For next nearest-neighbor hoppings which are between two **A** sites (or two **B** sites), $\mathbf{R}_2 - \mathbf{R}_1$ equals $\mathbf{d}_1 \equiv b(0,1)$, $\hat{C}_3\mathbf{d}_1$ or $\hat{C}_3^2\mathbf{d}_1$ (see main text Fig. 4(a)), the hopping phase factors are $e^{i(\mathbf{K}-\mathbf{K}')\cdot\mathbf{d}_1} = e^{i(\mathbf{K}-\mathbf{K}')\cdot\hat{C}_3\mathbf{d}_1} = e^{i(\mathbf{K}-\mathbf{K}')\cdot\hat{C}_3^2\mathbf{d}_1} = e^{i4\pi/3}$.

section S4. Exciton bands in superlattice potential: Exact solution and tight-binding model

Using Eqs. (S2) and (S3), the superlattice potential $V(\mathbf{R}) = E_g\big(\mathbf{r}_0(\mathbf{R})\big) + e\mathcal{E}d\big(\mathbf{r}_0(\mathbf{R})\big) - E_b$ for the interlayer excitons in the moiré can be expressed as

$$V(\mathbf{R}) = \left(E_{g,0} + e\mathcal{E}d_0 - E_b\right) + \left(\Delta E_{g,1} + e\mathcal{E}\Delta d_1\right)\left|f_0\left(\mathbf{r}_0(\mathbf{R})\right)\right|^2 + \left(\Delta E_{g,2} + e\mathcal{E}\Delta d_2\right)\left|f_+\left(\mathbf{r}_0(\mathbf{R})\right)\right|^2$$
$$= E_X(\mathcal{E}) + \sum_{n=1}^{3}\left(V(\mathcal{E})e^{i\mathbf{g}_n\cdot\mathbf{R}} + V^*(\mathcal{E})e^{-i\mathbf{g}_n\cdot\mathbf{R}}\right)$$

Here $V(\mathcal{E}) \equiv \frac{\Delta E_{g,1}+e\mathcal{E}\Delta d_1}{9} + \frac{\Delta E_{g,2}+e\mathcal{E}\Delta d_2}{9}e^{i2\pi/3}$, $E_X(\mathcal{E}) \equiv E_{g,0} + e\mathcal{E}d_0 - E_b + \frac{\Delta E_{g,1}+e\mathcal{E}\Delta d_1+\Delta E_{g,2}+e\mathcal{E}\Delta d_2}{3}$ and $\mathbf{g}_{1,2,3}$ are the three reciprocal lattice vectors of the moiré pattern as shown in fig. S7(a). The basis of momentum eigenstates in Eq. (S6) can be expressed in terms of the COM coordinate $\mathbf{R}$ and relative coordinate $\mathbf{r}_{\mathrm{eh}}$: $X_{\mathbf{Q}}(\mathbf{r}_{\mathrm{e}}, \mathbf{r}_{\mathrm{h}}) = e^{i(\mathbf{Q}+\mathbf{K}-\mathbf{K}')\cdot\mathbf{R}}U_{\mathbf{Q}}(\mathbf{R}, \mathbf{r}_{\mathrm{eh}})$, where

$$U_{\mathbf{Q}}(\mathbf{R}, \mathbf{r}_{\mathrm{eh}}) \equiv \sum_{\Delta\mathbf{Q}} e^{i\left(\Delta\mathbf{Q}+\frac{m_{\mathrm{h}}}{M_0}\mathbf{K}+\frac{m_{\mathrm{e}}}{M_0}\mathbf{K}'\right)\cdot\mathbf{r}_{\mathrm{eh}}}\Phi(\Delta\mathbf{Q})u_{\frac{m_{\mathrm{e}}}{M_0}\mathbf{Q}+\Delta\mathbf{Q},\mathrm{c}}\left(\mathbf{R}+\frac{m_{\mathrm{h}}}{M_0}\mathbf{r}_{\mathrm{eh}}\right)u^*_{-\frac{m_{\mathrm{h}}}{M_0}\mathbf{Q}+\Delta\mathbf{Q},\mathrm{v}}\left(\mathbf{R}-\frac{m_{\mathrm{e}}}{M_0}\mathbf{r}_{\mathrm{eh}}\right)$$

is a periodic function of $\mathbf{R}$ with the periodicity of moiré pattern, i.e., $U_{\mathbf{Q}}(\mathbf{R}+\mathbf{B}_m, \mathbf{r}_{\mathrm{eh}}) = U_{\mathbf{Q}}(\mathbf{R}, \mathbf{r}_{\mathrm{eh}})$ with $\mathbf{B}_m$ the lattice vector of the moiré superlattice. For excitons with low kinetic energies ($|\mathbf{Q}| \ll |\mathbf{K}|$), we can use the envelope approximation $u_{\frac{m_{\mathrm{e}}}{M_0}\mathbf{Q}+\Delta\mathbf{Q},\mathrm{c}} \approx u_{\Delta\mathbf{Q},\mathrm{c}}$ and $u_{-\frac{m_{\mathrm{h}}}{M_0}\mathbf{Q}+\Delta\mathbf{Q},\mathrm{v}} \approx u_{\Delta\mathbf{Q},\mathrm{v}}$ which imply that $U_{\mathbf{Q}} \approx U_{\mathbf{Q}=0}$.

The matrix element of $V(\mathbf{R})$ is

$$\langle X_{\mathbf{Q}'}|V(\mathbf{R})|X_{\mathbf{Q}}\rangle = E_X(\mathcal{E})\left(\sum_m e^{i(\mathbf{Q}-\mathbf{Q}')\cdot\mathbf{B}_m}\right)\int_{SC} U^*_{\mathbf{Q}'}(\mathbf{R}, \mathbf{r}_{\mathrm{eh}})e^{i(\mathbf{Q}-\mathbf{Q}')\cdot\mathbf{R}}U_{\mathbf{Q}}(\mathbf{R}, \mathbf{r}_{\mathrm{eh}})d\mathbf{R}d\mathbf{r}_{\mathrm{eh}}$$
$$+V(\mathcal{E})\sum_{n=1}^{3}\left(\sum_m e^{i(\mathbf{g}_n+\mathbf{Q}-\mathbf{Q}')\cdot\mathbf{B}_m}\right)\int_{SC} U^*_{\mathbf{Q}'}(\mathbf{R}, \mathbf{r}_{\mathrm{eh}})e^{i(\mathbf{g}_n+\mathbf{Q}-\mathbf{Q}')\cdot\mathbf{R}}U_{\mathbf{Q}}(\mathbf{R}, \mathbf{r}_{\mathrm{eh}})d\mathbf{R}d\mathbf{r}_{\mathrm{eh}}$$
$$+V^*(\mathcal{E})\sum_{n=1}^{3}\left(\sum_m e^{i(\mathbf{Q}-\mathbf{Q}'-\mathbf{g}_n)\cdot\mathbf{B}_m}\right)\int_{SC} U^*_{\mathbf{Q}'}(\mathbf{R}, \mathbf{r}_{\mathrm{eh}})e^{i(\mathbf{Q}-\mathbf{Q}'-\mathbf{g}_n)\cdot\mathbf{R}}U_{\mathbf{Q}}(\mathbf{R}, \mathbf{r}_{\mathrm{eh}})d\mathbf{R}d\mathbf{r}_{\mathrm{eh}}$$

where the integration $\int_{SC}(\cdots)d\mathbf{R}$ is restricted in a moiré supercell. Clearly, $\sum_m e^{i\mathbf{k}\cdot\mathbf{B}_m}$ is nonzero only when $\mathbf{k} = \mathbf{g}_l$ with $\mathbf{g}_l$ a general reciprocal lattice vector of the moiré superlattice. Meanwhile for small values of $|\mathbf{Q}|, |\mathbf{Q}'|, |\mathbf{g}_l| \ll |\mathbf{K}|$ we are interested, one can use the envelope approximation $U_{\mathbf{Q}'} \approx U_{\mathbf{Q}=0} \approx U_{\mathbf{Q}-\mathbf{g}_l}$ which leads to

$$\left(\sum_m e^{i\mathbf{g}_l\cdot\mathbf{B}_m}\right)\int_{SC} U^*_{\mathbf{Q}'}(\mathbf{R},\mathbf{r}_{\rm eh})e^{i\mathbf{g}_l\cdot\mathbf{R}}U_{\mathbf{Q}}(\mathbf{R},\mathbf{r}_{\rm eh})d\mathbf{R}d\mathbf{r}_{\rm eh}$$
$$=\int U^*_{\mathbf{Q}'}(\mathbf{R},\mathbf{r}_{\rm eh})e^{i\mathbf{g}_l\cdot\mathbf{R}}U_{\mathbf{Q}}(\mathbf{R},\mathbf{r}_{\rm eh})d\mathbf{R}d\mathbf{r}_{\rm eh}$$
$$=\int \left(e^{i(\mathbf{Q}-\mathbf{g}_l+\mathbf{K}-\mathbf{K}')\cdot\mathbf{R}}U_{\mathbf{Q}'}(\mathbf{R},\mathbf{r}_{\rm eh})\right)^*\left(e^{i(\mathbf{Q}+\mathbf{K}-\mathbf{K}')\cdot\mathbf{R}}U_{\mathbf{Q}}(\mathbf{R},\mathbf{r}_{\rm eh})\right)d\mathbf{R}d\mathbf{r}_{\rm eh}$$
$$\approx\int X^*_{\mathbf{Q}-\mathbf{g}_l}(\mathbf{r}_{\rm e},\mathbf{r}_{\rm h})X_{\mathbf{Q}}(\mathbf{r}_{\rm e},\mathbf{r}_{\rm h})d\mathbf{r}_{\rm e}d\mathbf{r}_{\rm h}=\delta_{0,\mathbf{g}_l}$$

The above last step comes from the orthonormality of the momentum eigenstates. So $\langle X_{\mathbf{Q}'}|V(\mathbf{R})|X_{\mathbf{Q}}\rangle \approx E_X(\mathcal{E})\delta_{\mathbf{Q},\mathbf{Q}'}+\sum_{n=1}^{3}\left(V(\mathcal{E})\delta_{\mathbf{g}_n+\mathbf{Q},\mathbf{Q}'}+V^*(\mathcal{E})\delta_{-\mathbf{g}_n+\mathbf{Q},\mathbf{Q}'}\right)$

Therefore, under this basis of momentum eigenstates, the Hamiltonian $\widehat{H}_T$ for the exciton COM motion consists of the diagonal Stark shift and kinetic energy term $E_X(\mathcal{E})+\frac{\hbar^2|\mathbf{Q}|^2}{2M_0}$, and the off-diagonal terms due to the superlattice potential $V(\mathbf{R})$. Write $\mathbf{Q}=\mathbf{g}_l+\mathbf{q}$, where $\mathbf{g}_l$ is a general reciprocal lattice vector of the moiré superlattice, and $\mathbf{q}$ is a wave vector within the hexagonal moiré-BZ, we have $\widehat{H}_T=\sum_{\mathbf{q}}\widehat{H}_{\mathbf{q}}$, where

$$\widehat{H}_{\mathbf{q}}=\sum_l\left[\left(E_X(\mathcal{E})+\frac{\hbar^2|\mathbf{g}_l+\mathbf{q}|^2}{2M_0}\right)|\mathbf{g}_l+\mathbf{q}\rangle\langle\mathbf{g}_l+\mathbf{q}|+\sum_{n=1,2,3}\left(V(\mathcal{E})|\mathbf{g}_l+\mathbf{g}_n+\mathbf{q}\rangle\langle\mathbf{g}_l+\mathbf{q}|+h.c.\right)\right]$$

The exciton dispersion can then be numerically solved by dropping those $\mathbf{g}_l$ with large magnitude that exceed some cutoff value ($|\mathbf{g}_l|>g_{\rm max}$). For $b<20$ nm, we find the low energy bands converge well for a cutoff value $g_{\rm max}=\frac{16\pi}{\sqrt{3}b}$. The several lowest exciton bands of a $b=10$ nm moiré superlattice is shown in Fig. 4(c) in the main text.

On the other hand, one can also describe the two lowest exciton bands with an effective tight-binding model following the standard approach in optical lattices (*35*). In a honeycomb optical lattices with same potential profile as $V(\mathbf{R})$, Ref. (*35*) has shown that it is sufficient to keep up to third nearest-neighbor hopping terms. The difference here lies in the complex hopping phases which have already been fully determined as discussed in Section III above, while the magnitudes of the hopping strengths $t_{0,1,2}\equiv\left|t\left(\mathbf{d}_{0,1,2}\right)\right|$ can be obtained by fitting the numerical results

(shown as the symbols in fig. S7(b)). Ref. (*35*) has also given the following fitting forms for the hopping strength

$$t_0 \approx 1.16E_R\left(\frac{V}{E_R}\right)^{0.95}\exp\left[-1.634\sqrt{\frac{V}{E_R}}\right],$$
$$t_1 \approx 0.78E_R\left(\frac{V}{E_R}\right)^{1.85}\exp\left[-3.404\sqrt{\frac{V}{E_R}}\right], \qquad \text{(S15)}$$
$$t_2 \approx 1.81E_R\left(\frac{V}{E_R}\right)^{2.75}\exp\left[-5.196\sqrt{\frac{V}{E_R}}\right]$$

Here $E_R = \frac{\hbar^2}{2M_0}\left(\frac{4\pi}{3b}\right)^2$ is the recoil energy, $V \approx 10$ meV is the barrier height. $t_{0,1,2}$ as functions of b from Eq. (S15) are shown as curves in Fig. 3(f) in the main text and fig. S7(b). By comparing with the fitting of the exact exciton bands, we can see that for $V/E_R > 3$, Eq. (S15) agree well with those from fitting the numerical results, but they underestimate the magnitudes of $t_{0,1,2}$ for smaller V/E_R.

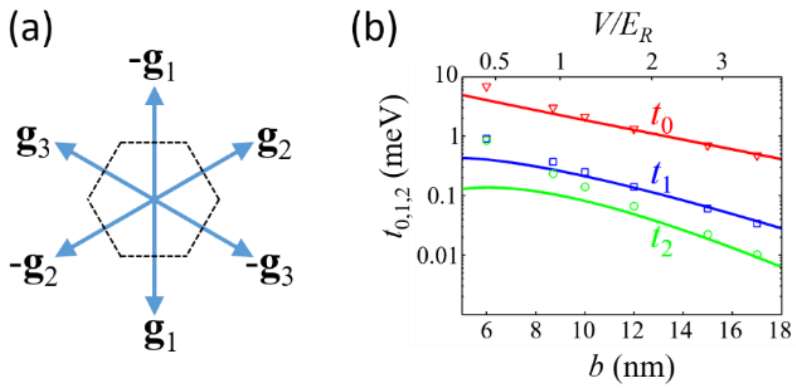

fig. S7. The six reciprocal lattice vectors in the Fourier components of the excitonic potential, and the obtained hopping magnitudes $t_{0,1,2}$ as functions of the moiré period b or V/E_R. (a) The Fourier components of the excitonic potential correspond to six reciprocal lattice vectors $\pm\mathbf{g}_n$ (n=1,2,3). The dashed hexagon is the moiré superlattice BZ. (b) The obtained magnitudes of $t_{0,1,2}$ as functions of the moiré period b or V/E_R. The symbols are the fits to the numerical results under $\mathcal{E} = \mathcal{E}_0$, while the curves are the asymptotic forms Eqs. (S15). For b~10 nm or smaller, Eqs. (S15) underestimate $t_{0,1,2}$.

section S5. Exciton-exciton interactions in the superlattices

We now consider the on-site Coulomb interaction $\hat{V}_C$ between two exciton wavepackets located in the same nanodot (e.g., at **A**)

$$U = \langle \mathcal{X}\mathcal{X}|\hat{V}_C|\mathcal{X}\mathcal{X}\rangle = \sum_{\mathbf{Q}_1\mathbf{Q}_2\mathbf{Q}_3\mathbf{Q}_4} e^{i(\mathbf{Q}_3+\mathbf{Q}_4-\mathbf{Q}_1-\mathbf{Q}_2)\cdot\mathbf{R}} W(\mathbf{Q}_3)W(\mathbf{Q}_4)W(\mathbf{Q}_1)W(\mathbf{Q}_2)\langle X_{\mathbf{Q}_3}X_{\mathbf{Q}_4}|\hat{V}_C|X_{\mathbf{Q}_1}X_{\mathbf{Q}_2}\rangle$$

Here $\langle X_{\mathbf{Q}_3}X_{\mathbf{Q}_4}|\hat{V}_C|X_{\mathbf{Q}_1}X_{\mathbf{Q}_2}\rangle$ is the Coulomb matrix element between momentum eigenstates, which has been thoroughly investigated for spatially direct and indirect excitons in early papers (*52-55*). It is shown that for $|\mathbf{Q}_{1,2,3,4}| \lesssim w^{-1} \ll a_B^{-1}$, $\langle X_{\mathbf{Q}_3}X_{\mathbf{Q}_4}|\hat{V}_C|X_{\mathbf{Q}_1}X_{\mathbf{Q}_2}\rangle \approx \delta_{\mathbf{Q}_1+\mathbf{Q}_2,\mathbf{Q}_3+\mathbf{Q}_4}\frac{a_B^2}{S}V_C$,where a_B is the exciton Bohr radius and S the box normalization area. V_C is a constant with two contributions (*52-55*): (i) V_{ex}, from the exchange interaction between excitons with the same spin indices only, and (ii) V_{dd}, from the dipole-dipole interaction independent of the spin indices. Following (*17, 56*), we estimate that $V_{\mathrm{ex}}\sim E_b$ and $V_{\mathrm{dd}}\sim\frac{d}{a_B}E_b$. So

$$U_{\mathrm{ex/dd}} = V_{\mathrm{ex/dd}}\frac{a_B^2}{S}\left(\frac{4\pi}{S}\right)^2 w^4 \sum_{\mathbf{Q}_1\mathbf{Q}_2\mathbf{Q}_3} e^{-\frac{w^2}{2}(\mathbf{Q}_1^2+\mathbf{Q}_2^2+\mathbf{Q}_3^2+(\mathbf{Q}_1+\mathbf{Q}_2-\mathbf{Q}_3)^2)} = \frac{1}{2\pi}\left(\frac{a_B}{w}\right)^2 V_{\mathrm{ex/dd}} \qquad \text{(S16)}$$

In the last step we have converted the summation into integral: $\sum_{\mathbf{Q}}(\ldots) = \frac{S}{(2\pi)^2}\int(\ldots)d\mathbf{Q}$. Using the parameters d = 0.6 nm, a_B = 2 nm, w = 0.3b, E_b = 0.2 eV, we estimate $U_{\mathrm{ex}} = \frac{1}{2\pi}\left(\frac{a_B}{w}\right)^2 V_{\mathrm{ex}}\sim$14 meV and $U_{\mathrm{dd}} = \frac{1}{2\pi}\left(\frac{a_B}{w}\right)^2 V_{\mathrm{dd}}\sim$4 meV for b = 10 nm. With the change of b, we have $U_{\mathrm{ex}}\sim\left(\frac{10\text{ nm}}{b}\right)^2\times$ 14 meV and $U_{\mathrm{dd}}\sim\left(\frac{10\text{ nm}}{b}\right)^2\times$ 4 meV.